Effects of Wavelength and Defect Density on the Efficiency of (In,Ga)N-Based Light-Emitting Diodes

Markus Pristovsek,[*] An Bao, and Rachel A. Oliver
Department of Materials Science and Metallurgy, University of Cambridge, 27 Charles Babbage Road, Cambridge CB3 0FS, United Kingdom

Tom Badcock,[†] Muhammad Ali,[‡] and Andrew Shields
Toshiba Research Europe Ltd., Cambridge Research Laboratory, 208 Science Park, Milton Road, Cambridge CB4 0GZ, United Kingdom
(Received 7 March 2017; published 5 June 2017)

We measure the electroluminescence of light-emitting diodes (LEDs) on substrates with low dislocation densities (LDD) at 10^6 cm^{-2} and low 10^8 cm^{-2}, and compare them to LEDs on substrates with high dislocation densities (HDD) closer to 10^{10} cm^{-2}. The external quantum efficiencies (EQEs) are fitted using the ABC model with and without localization. The nonradiative-recombination (NR) coefficient A is constant for HDD LEDs, indicating that the NR is dominated by dislocations at all wavelengths. However, A strongly increases for LDD LEDs by a factor of 20 when increasing the emission wavelength from 440 to 540 nm. We attribute this to an increased density of point defects due to the lower growth temperatures used for longer wavelengths. The radiative recombination coefficient B follows the squared wave-function overlap for all samples. Using the observed coefficients, we calculate the peak efficiency as a function of the wavelength. For HDD LEDs the change of wave-function overlap (i.e., B) is sufficient to reduce the EQE as observed, while for LDD LEDs also the NR coefficient A must increase to explain the observed EQEs. Thus, reducing NR is important to improving the EQEs of green LEDs, but this cannot be achieved solely by reducing the dislocation density: point defects must also be addressed.

DOI: 10.1103/PhysRevApplied.7.064007

I. INTRODUCTION

Many efforts are under way to improve the external quantum efficiency (EQE) of (In,Ga)N-based light-emitting diodes (LEDs). Currently, such LEDs are usually produced either on (0001) sapphire or (111) silicon substrates by heteroepitaxy. This typically results in a threading dislocation density (TDD) of low 10^8 cm^{-2} on sapphire and closer to 10^9 cm^{-2} on silicon. The variation in TDD has an impact on the EQE, which is shown for LEDs emitting at wavelengths shorter than 460 nm [1–6].

Apart from the TDD, the efficiency of nitride LEDs decreases at wavelengths longer than 480 nm. This is often referred to as the "green gap." One explanation which is often put forward is a slower radiative recombination rate due to a reduced overlap between the electron and hole-wave function which is caused by a larger piezoelectric field from a larger strain with higher In content. However, recent reports on LEDs [7], laser diodes [8], and photoluminescence (PL) of quantum wells (QWs) [9,10] found that nonradiative recombination also increases at longer wavelengths. A comparison of QWs with the same wavelength and structural parameters but grown at different temperatures shows that the resulting internal quantum efficiency (IQE) strongly depends on growth temperature. This suggests that nonradiative losses are not strain driven [10,11].

In order to quantify the influence of wave-function overlap and TDD on nonradiative recombination and the green gap, we investigate LEDs over a wide wavelength range, using three different basic templates with very different dislocation densities. The obtained coefficients are used to model the EQE of LEDs with different dislocation densities to provide an insight into the origin of the green gap.

II. EXPERIMENTAL

All the LEDs are grown by metal-organic vapor-phase epitaxy. The lowest dislocation density is for freestanding GaN substrates, obtained from Kyma technologies. Low dislocation-density (LDD) templates are grown on (0001) sapphire with an optimized low-temperature nucleation around 530 °C, followed by annealing at 1050 °C.

[*]Present address: Center for Integrated Research of Future Electronics, Institute for Materials and Systems for Sustainability, Nagoya University, 1 Furo-cho, Chikusa-Ku, Nagoya 464-8603, Japan.
pristovsek@nagoya-u.ac.jp
[†]Present address: Oclaro Technology Ltd., Caswell, Towcester NN12 8EQ, United Kingdom.
[‡]Present address: Osram Opto Semiconductors GmbH, Leibnizstr. 4, 93055 Regensburg, Germany.

 © 2017 American Physical Society

Growth is initiated by conditions which encourage the formation of three-dimensional islands, followed by island coalescence as described in Ref. [12]. For high dislocation-density (HDD) samples the nucleation and annealing times are shortened, and conditions are used which promote two-dimensional growth after the annealing step [12]. TDDs are obtained from the density of dark spots in scanning-electron-microscope cathodoluminescence (SEMCL) for freestanding GaN and LDD, while for the HDD growth the TDD-related surface pits are counted in atomic force microscopy [13]. Typical TDDs are below 10^7 cm^{-2} for freestanding GaN, 2–4 × 10^8 cm^{-2} for LDD, and close to 10^{10} cm^{-2} for HDD.

For the HDD LEDs the thickness of the n-doped side is limited to 1 μm, because thicker layers crack due to high (10^{-3}) in-plane tensile strain, as determined by x-ray diffraction (XRD). Hence, to maintain a comparable LED structure, the thickness of the n-doped side is limited to 1.5 μm for the LEDs on freestanding GaN and LDD. In order to span a wavelength range from blue to green without changing the nominal structure, only three quantum wells (QWs) are used. QW growth is carried out entirely with nitrogen-carrier gas and trimethylindium and triethylgallium precursors. The GaN barriers are grown under a 99:1 nitrogen-hydrogen mixture about 80 °C higher than the QWs, and the temperature is increased immediately after the end of the QW. This so-called two-temperature strategy [14] minimizes the formation of trench defects at longer emission wavelengths which may otherwise control the EQE [15]. Indeed, we observe fewer than 10^7 cm^{-2} trench defects and no change in TDD for multiple QWs (MQWs) without a p-GaN cap emitting at 545 nm by SEMCL. XRD shows fully strained layers in reciprocal space maps. TEM shows QWs with few thickness fluctuations and nice interfaces. No dislocations are generated in the MQWs, even in the LED at 532 nm on the freestanding GaN template.

No electron blocking layer is used; the last barrier is covered with 140 nm of p-GaN and 20 nm of $p++$ GaN, grown at the relatively low susceptor surface temperature of 900 °C. The LEDs are processed into devices with five different p-contact geometries in different sizes, using Ni/Au transparent contact (4.5/4.5 nm annealed at 450 °C in $O_2 + N_2$ for 5 min) with Ti/Au pads (20/80 nm) as p contacts and Ti/Al/Ti/Au (15/50/30/80 nm annealed at 700 °C in N_2 for 60 s) as n contacts. The electroluminescence (EL) is measured on chip by backside collection using an integrating sphere with two different detectors, or from the front using an optical fiber. For each wavelength and template at least four different devices are measured and analyzed.

The wave-function overlap integral is calculated as described in Ref. [16], assuming a bowing parameter of 1.7 and a QW thickness of 3.0 nm.

III. RESULTS AND DISCUSSION

A. Theory

The emission of LEDs is commonly described by the ABC model [7,17–19]. The current I is connected to the carrier density n by

$$N(n) := I(n)\frac{\eta_{\mathrm{inj}}}{e_0 V} = (An + Bn^2 + Cn^3), \tag{1}$$

where N is the total recombination rate, the coefficient A is attributed to the Shockley-Read-Hall (SRH) nonradiative recombination, B gives the radiative free carrier (electron + hole) recombination, and C is the carrier-activated loss (often assumed to be Auger related). V, the volume of the active region, is given by $V = dS$, where d is the thickness of the QW, S is the area of the device, e_0 is the elementary charge, and η_{inj} is the injection efficiency.

For the analysis, we assume that the light output is only given by the radiative recombination. Optical losses between the QW and the detector are accounted for by the extraction efficiency $\eta_e \le 1$. Then the light output L (the number of emitted photons per time) is given by the radiative recombination rate in the active volume

$$L(n) = \eta_e V B n^2. \tag{2}$$

The EQE is defined as the number of photons detected divided by the number of injected carriers

$$\mathrm{EQE}(n) = L(n)\frac{e_0}{I(n)} = \eta_e \eta_{\mathrm{inj}} \frac{Bn^2}{An + Bn^2 + Cn^3}. \tag{3}$$

For $\eta_e = \eta_{\mathrm{inj}} = 1$ the EQE is identical to the internal quantum efficiency (IQE). In Eq. (3) any increase of the coefficients A or C would reduce the peak (maximum) EQE. From theory, a higher TDD should increase A, because the SRH recombination only depends on the density of nonradiative centers and the carrier density. The other loss C is a three-carrier process ($\propto n^3$). As such it is only relevant when there is a high local carrier density, at which point the SRH recombination centers will be mostly saturated. Therefore, C is expected to be largely independent of the TDD. Indeed, experimentally C is nearly constant over a large wavelength range [7] or various In contents and QW thicknesses [20].

The most important process is the radiative emission. Its coefficient B is related to the square of the wave-function overlap [7], which is determined by the In content in the QW and the barrier, the QW thickness, and the substrate orientation. If free carriers recombine when they randomly meet, the radiative recombination is proportional to the product of electron and hole densities n^2. However, electrons can be localized at QW thickness fluctuations or holes at random alloy fluctuations [21]. Then, the

electron and hole are captured subsequently and the radiative recombination becomes proportional to the carrier density n, i.e., the chance of a carrier meeting a localization site. In the localized case, the number of generated photons is $\eta_e V B_l n$ (where B_l is the localized recombination rate), and the EQE becomes

$$\mathrm{EQE} = \eta_e \eta_{\mathrm{inj}} \frac{B_l n}{An + B_l n + Cn^3}, \tag{4}$$

assuming the carrier-activated loss still scales like n^3.

Figure 1 shows the obtained EQE curves. With localization the EQE has its maximum at zero carrier density with $\mathrm{EQE}(0) = \eta_e \eta_{\mathrm{inj}} B_l/(A + B_l)$ (since nonradiative as well as radiative recombination are both linear in n). At higher carrier densities the additional Auger losses start to reduce the localized EQE. On the other hand, without localization the EQE goes to zero for small carrier densities. If both recombination processes occur simultaneously, then localization will dominate at low carrier densities.

An earlier time-dependent PL study found that localization could be only modeled reasonably well if either an excess of holes or electrons are localized [22]. Thus, it is no surprise that the shape of the EQE for the sum of both recombination processes in Fig. 1 (solid) is very similar to the EQE obtained by background doping [19,23], i.e., when one carrier type is in abundance. For background doping the radiative recombination becomes $\propto n$ at low carrier densities. For typical *ABC* coefficients Karpov *et al.* estimated that an excess (i.e., localization site density) of 5×10^{18} cm^{-3} is needed to dominate recombination up to the maximum EQE (Fig. 3 in Ref. [23]). This rather high number of localization sites explains why typical EQE curves are closer to the classical EQE shape.

Mathematically, fitting an experimental EQE with a combination of Eqs. (3) and (4) is difficult, since A and B_l are strongly interdependent. But Fig. 1 also shows that even for a large B_l the shape can still be approximated by the nonlocalized classical Eq. (3) for carrier densities starting shortly before the maximum EQE, although this slightly overestimates A. Thus, if there is still a clear maximum, then the EQE curve can be described with a small error by Eq. (3) around the maximum.

A fundamental assumption of the *ABC* model is that the three coefficients A, B, and C are constant. However, there are recent indications that this is not necessarily the case. For instance, the nonradiative lifetime (inverse of A) increases with increasing carrier density [24–26]. Also, the radiative recombination is expected to increase at high current densities, when screening of the internal fields in the QW increases the wave-function overlap (and thus B). Other effects compete with this, namely, carrier-activated defect recombination [27] or hole degeneration in QWs [23]. (The latter reduces B by hole degeneration $\propto \{[1 - \exp(-n/D)]/n\tau_r\}$, with D the density of states in the QW, and τ_r the radiative lifetime [23].) Furthermore, even the injection efficiency η_{inj} decreases at high carrier densities [28,29]. Since all these effects compete, the classical *ABC* model (assuming constant coefficients) reaches its limits at high carrier densities. Still, the *ABC* model fits the experimental EQE curves of many LEDs very well around the EQE maximum. Within the limitations of the model, analysis of the systematic variation of the A, B, and C coefficients should facilitate further understanding of the green gap.

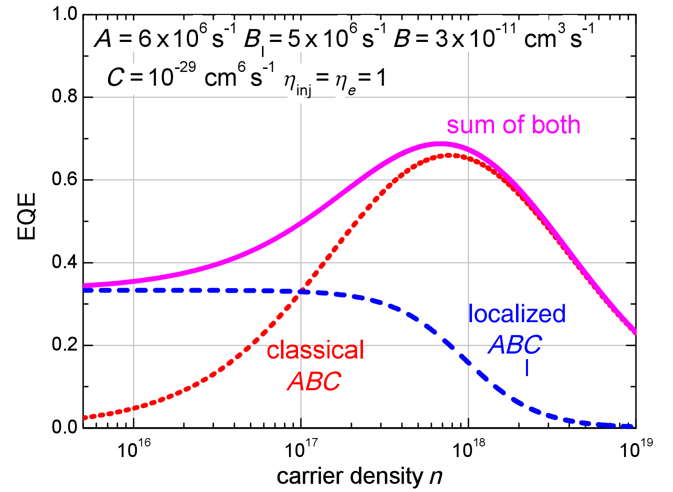

FIG. 1. Shape of EQE curves for the classical case with $L \propto n^2$ [Eq. (3), dotted] and the localized case with $L \propto n$ [Eq. (4), dashed] and a combination of both for typical coefficients.

A direct fitting of the EQE with Eq. (3) is not possible, since the carrier density is given by $\sqrt{L} = \sqrt{\eta_e B} n$, but neither B nor η_e are known. Since the light output is proportional to the carrier density squared, one defines the new independent variable $x = \sqrt{L/L_{\mathrm{peak}}}$ with L_{peak} the light output at maximum EQE. By also defining $P = (B/\sqrt{AC})$ and rearranging Eq. (3) [18] one finally obtains

$$\frac{\mathrm{EQE}(x)}{\mathrm{EQE}_p} = \frac{P + 2}{P + \frac{1}{x} + x}. \tag{5}$$

The three fitting parameters are very independent, the shape is entirely given by P, the amplitude is EQE_p, and the maximum position is L_{peak}, and there is very little cross coupling between these.

From P the maximum $\mathrm{IQE}_{\mathrm{peak}}$ can be calculated

$$\mathrm{IQE}_{\mathrm{peak}} = \frac{P}{P + 2} = \frac{B}{B + \sqrt{AC}} \tag{6}$$

and from that follows the extraction and injection efficiencies

$$\eta_e\eta_{\rm inj} = \frac{1}{{\rm IQE}_{\rm peak}{\rm EQE}_p} = \frac{P+2}{P{\rm EQE}_p}. \qquad (7)$$

At $\mathrm{IQE_{peak}}$, the first derivate of Eq. (3) is zero, i.e., $(d/dn)\mathrm{EQE} = 0$. The only meaningful solution is

$$n_{\rm peak} = \sqrt{\frac{A}{C}}, \qquad (8)$$

which can be put into Eqs. (1) and (3) to obtain values for the coefficient A, B, or C when fixing one of them. Using $N_{\rm peak} = N(n_{\rm peak}) = I_{\rm peak}(\eta_{\rm inj}/e_c V)$ one obtains finally

$$N_{\rm peak}(1-{\rm IQE}_{\rm peak}) = 2\frac{N_{\rm peak}}{P+2} = 2\sqrt{\frac{A^3}{C}},$$
$$\frac{N_{\rm peak}}{4}\frac{(1-{\rm IQE}_{\rm peak})^2}{{\rm IQE}_{\rm peak}} = \frac{N_{\rm peak}}{P(P+2)} = \frac{A^2}{B}, \qquad (9)$$

or as dependence from C

$$\frac{4N_{\rm peak}({\rm IQE}_{\rm peak})^3}{(1-{\rm IQE}_{\rm peak})^2} = \frac{N_{\rm peak}P^3}{P+2} = \frac{B^3}{C^2}. \qquad (10)$$

For very low excitation one can neglect the C term in Eq. (1) completely: $I \approx (e_0 V/\eta_{\rm inj})(An + Bn^2)$. From Eq. (2) one can express the carrier density by the light output $n = \sqrt{L/(\eta_e BV)}$ and replace I by Le_0/EQE [Eq. (3)]. With this one obtains

$$\frac{1}{\rm EQE} \approx \frac{1}{\eta_{\rm inj}\eta_e} + \frac{A}{\eta_{\rm inj}}\sqrt{\frac{V}{\eta_e BL}}. \qquad (11)$$

This was first derived by Opdorf and 't Hooft [30]. Fitting a line to the low current data of EQE^{-1} over $L^{-1/2}$ gives the slope and the intercept. The latter is the reciprocal of $\eta_e\eta_{\rm inj}$, although the η_e is about a factor of 2 smaller compared to Eq. (7), since it is obtained by extrapolating to large currents, where nonlinear C losses cannot be neglected. This method works best for $L \ll L_{\rm peak}$, more than a factor of 100 away from the peak EQE, and one has to be careful that the device does not show localization.

In Eq. (11), the slope sl is given by $(A/\eta_{\rm inj})\sqrt{V/(\eta_e B)}$. Rearranging this we get

$$\frac{\eta_{\rm inj}^2\eta_e}{V}{\rm sl}^2 = \frac{A^2}{B}, \qquad (12)$$

which can be directly compared with Eq. (9). Indeed, Eqs. (12) and (9) give similar values when using the same η_e and $\eta_{\rm inj}$. The method does not rely on the C coefficient, which is important since there is some disagreement about the value of C in the literature (as discussed in the next section).

Equations (9), (10), or (12) require prior knowledge of B to calculate the other coefficients A and C. An independent way to obtain B is first described by Eliseev *et al.* [31]. It uses frequency-dependent small-signal-modulated EL to obtain the differential carrier lifetime τ: The derivative of Eq. (1) to n is $(1/\tau) = [(\partial N)/\partial n] = A + 2Bn + 3Cn^2$. For small carrier densities ($I \ll I_{\rm peak}$) one can ignore the Cn^2 term, and after squaring one obtains $\tau^{-2} = A^2 + 4B(An + Bn^2)$. Since $(An + Bn^2)$ is proportional to the injected current in this regime, then τ is given by $\tau^{-2} = A^2 + (4B\eta_{\rm inj}I)/(e_0 V)$. Thus from measurements at different currents, one can get B from the first derivative to the current I

$$B = \frac{e_0 V}{4\eta_{\rm inj}}\frac{\partial}{\partial I}\tau^{-2} \qquad (13)$$

using the same volume V and injection efficiency $\eta_{\rm inj}$ as before.

This leaves us with the last unknown, the injection efficiency $\eta_{\rm inj}$. Calculations have shown that $\eta_{\rm inj} > 90\%$ is realistic for 480 nm MQWs at low excitation close to $\mathrm{IQE_{peak}}$ but decreases at higher currents [28,29] and also decreases at higher temperatures or with single QWs [32]. Thus, a constant $\eta_{\rm inj}$ is a reasonable assumption at the small current densities for MQWs as in our study. So we quantify $\eta_{\rm inj}$ by assuming an ideal injection for the sample with the largest $\eta_e\eta_{\rm inj}$ in our wavelength series. Any reduction in $\eta_e\eta_{\rm inj}$ is then solely assigned to a decrease of $\eta_{\rm inj}$. Thus, when comparing to other experimental results, one should allow for a scaling of

$$A' = \sqrt{k}A, \qquad B' = kB, \qquad C' = k^{3/2}C, \qquad (14)$$

with a scaling constant k due to uncertainties in active volume and peak injection efficiency of the reference sample.

B. Results

The first parameter to determine is the volume of the active region. Since the extracted mean QW thicknesses from TEM agreed well with the values from XRD, we will use a width of 3 nm per QW for all samples. Since there are three QWs in the LEDs the total thickness is 9 nm. While most publications use the same approach, some assume a smaller active region due to the smaller region with a high wave-function overlap (e.g., Ref. [33]). Furthermore, the carrier density in all QW may be not equal and thus also altering the effective thickness used for calculating the carrier densities. Hence, there is already a systematic deviation of the absolute values of the ABC coefficients in the literature from the different definitions of the active region.

Figure 2 shows typical measured EQE curves at different wavelengths and their fits using Eq. (5). Most deviations between measurements and fits are found at low currents,

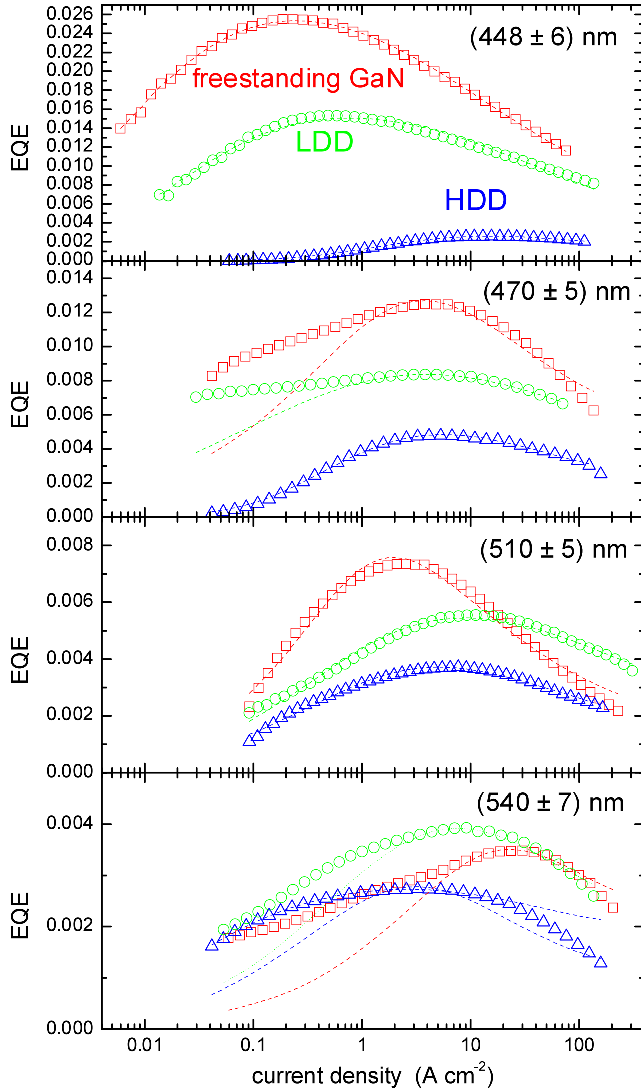

FIG. 2. EQE curves as a function of current density, measured on chip at four different wavelengths on freestanding GaN (square), LDD (circle), and HDD (triangle). Dotted lines are the fits using Eq. (5) and converted back to J. The divisions of the y axis are always 0.002 arbitrary units. For the longest wavelength LEDs (bottom) the shapes strongly deviate from the ideal ABC curve as both fits of emphasizing the low current end (dashed) or of the high-current end (dotted) are not good.

e.g., in Fig. 2 for the freestanding and LDD at 470 nm. These EQEs could be simulated by assuming localization [Eq. (4), see Fig. 1], although then A and B_l become interdependent and a unique combination of coefficients cannot be obtained. If one instead starts the fitting at slightly higher currents closer to the EQE maximum, then these EQEs can be still fitted with Eq. (5).

At the longest wavelength, above 540 nm, the EQE curves are very broad, with an asymmetric maximum, and sometimes even a second shoulder at lower currents, as well as strong localizationlike shape. While a broad maximum would correspond to a high IQE, the detected absolute light output is rather low. Moreover, the entire shape of the curve is not fitted well. Therefore, we may have reached the usable limits of the ABC model at 540 nm, as discussed before.

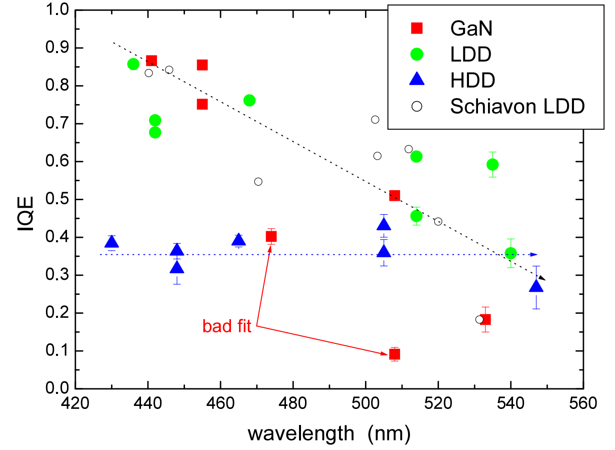

FIG. 3. Mean peak IQE from fitting and Eq. (6). The bars are the statistical errors from measuring all devices at that wavelength. The circles are LDD LEDs on sapphire by Schiavon *et al.* [7] and calculated from the A, B, and C coefficients using Eq. (6).

Despite the deviations, the fitting is successful for most of the LEDs at shorter wavelengths: There are only two device series, where the peak IQE strongly deviates from the trend (in Fig. 3 on freestanding GaN at 472 nm and one contact geometry at 508 nm). In both of these cases the fit at low and at high currents deviate and thus affect the fitted IQE. Otherwise, the peak IQE in Fig. 3 from the fitting shows the same wavelength-dependent trends as seen in the EQE curves in Fig. 2, i.e., the peak IQE-EQE is decreasing towards green, and the current density at maximum EQE is shifted to higher currents for lower EQEs.

Figure 4(a) shows the combined efficiency $\eta_e \eta_{\mathrm{inj}}$ from the fitting. Since the structures of all LEDs are similar, the extraction efficiency η_e is expected to be almost constant. Only self-adsorption in the p-GaN may somewhat reduce η_e towards longer wavelengths. However, most other losses like carrier bypassing the QW at V defects and other QW defects, nonuniform injection, or carrier overflow will reduce the injection efficiency η_{inj}. Since the latter is needed for further analysis, we conservatively assume a wavelength-independent extraction efficiency η_e given by the maximum of $\eta_e \eta_{\mathrm{inj}}$ for each template type. Then any reduction of $\eta_e \eta_{\mathrm{inj}}$ is due to injection losses. The so-obtained injection efficiencies η_{inj} have their peak value in Fig. 4(b) around 450 nm. Since our LEDs neither had an electron blocking layer nor an (In,Ga)N underlayer below the QWs, the reduction of η_{inj} at shorter wavelengths is probably caused by QWs which become too shallow for efficient injection and carriers start to overflow. A similar reduction of η_{inj} has been reported when the internal fields are reduced in semipolar QWs [34]. As mentioned before, the reduction of η_{inj} towards longer wavelengths is likely

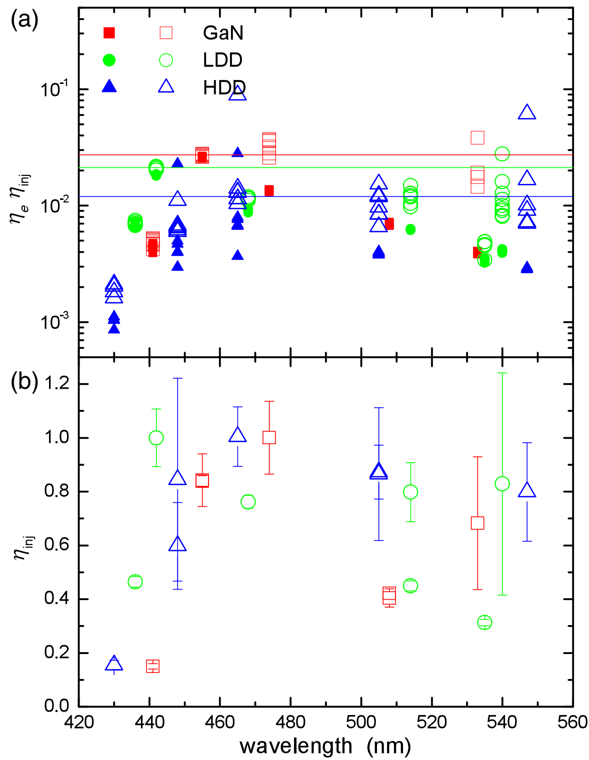

FIG. 4. (a) Efficiencies $\eta_e\eta_{inj}$ from Eq. (7) with their mean peak value indicated as lines. (b) Injection efficiencies η_{inj} assuming that the reduction to the peak value is only caused by a reduced injection efficiency.

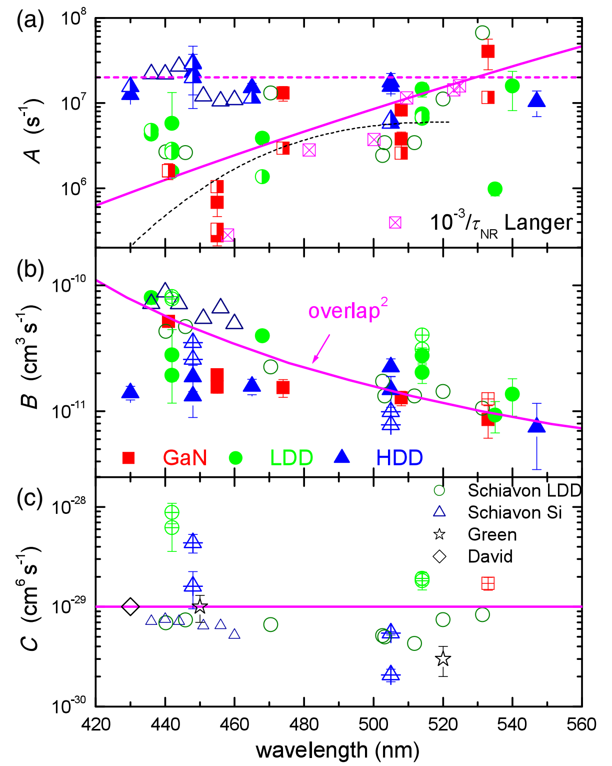

FIG. 5. *ABC* coefficient points assuming $C = 10^{-29}$ cm^6 s^{-1} on freestanding GaN (filled square), LDD (filled circle), and HDD (filled triangle) or open symbols for coefficients for LDD on sapphire (open square) and HDD-like on Si (open triangle) from Schiavon *et al.* [7], both shifted by $k = 16$ as in Eq. (14). The thick solid and dotted lines mark the ideal dependence of *A*, *B*, and *C* which is used to model HDD-LDD LED IQEs. (a) Extracted coefficient *A* from Eq. (9). The freestanding GaN-LDD *A* increase similar to the reverse nonradiative lifetimes (⊠) of $5 \times$ QWs from Langer *et al.* [9], and also follow the calculated *A* coefficients for nonradiative recombination at gallium vacancy-oxygen complexes (black dashed line from Alkauskas *et al.* [35]). The half-filled symbols are calculated using Eq. (12). (b) Extracted coefficients *B* from Eq. (10) or directly from differential carrier lifetimes (⊞ ⊕ ⊕) using Eq. (13). The line is the squared overlap between electron and hole-wave functions for 3.0 nm QWs normalized to 1.5×10^{-11} cm^3 s^{-1} at 500 nm. (c) Extracted *C* coefficient from differential carrier lifetimes and Eq. (10), the stars are from [36], and diamonds from [37].

caused by η_e due to self-adsorption in the *p*-GaN, i.e., to a reduced extraction efficiency η_e. However, its variation is small compared to the one of the *A* or *B* coefficients.

Now, we can finally derive values for *A*, *B*, and *C*. First, we calculate *B* using Eq. (13) from the modulated EL measurements at low current densities [crossed symbols in Fig. 5(b)]. Because localization has the strongest impact at low carrier densities (as discussed), this technique works only for a few devices and contact geometries. The resulting *B* coefficients are mostly in the range of $1\text{–}4 \times 10^{11}$ cm^3 s^{-1}, which is a commonly reported range [4,20,33]. $B = 6 \times 10^{11}$ cm^3 s^{-1} is reported for a green LED using the same technique [31].

Putting the obtained *B* into Eq. (10) yields the *C* coefficients in Fig. 5(c), which scatter around 10^{-29} cm^6 s^{-1} with no clear wavelength dependence. A nearly wavelength-independent *C* is observed in the literature using direct fitting [20], or the high current differential carrier lifetimes [7,36,37]. In the literature, the *C* coefficient is often reported around 10^{-29} cm^6 s^{-1} for measurements on MQWs structures [31,36,37] and $< 10^{-31}$ cm^6 s^{-1} for single QWs [7,29]. Since all of these values are obtained from modulation measurement, the most likely explanation is a nonuniform carrier distribution among the MQWs especially at low currents, which results in a larger apparent *C* coefficient for MQWs. Since we measured MQWs and furthermore focus on the *A* and *B* coefficients, the absolute value of *C* is not critical: It just scales *A* and *B* according to Eq. (14) but gives the same EQE. Therefore, we choose $C = 10^{-29}$ cm^6 s^{-1} to calculate *A* and *B* from Eq. (9). Since we use a different *C* value, in the following the single QW results of Schiavon *et al.* are scaled by $k = 16$ using Eq. (14). Again, the scaling has no impact for the analysis in this paper on the contribution of *A* and *B* to the green gap. Furthermore, Eq. (12) allows us to determine *A* only from *B*, and those values are consistent with the *A* calculated from Eq. (9).

The obtained *A* coefficients in Fig. 5(a) are almost constant for high-defect densities (HDD) at a level slightly

above 10^7 s^{-1}. They are also close to the values for the GaN on Si LEDs [△ in Fig. 5(a)], which had about 6 times higher dislocation densities than the LDD ones [7]. For the LDD LEDs either on freestanding GaN or LDD on sapphire, the A coefficients steeply increase from below 10^6 s^{-1} at 440 nm to 2×10^7 s^{-1} at 530 nm. Again, a similar trend is visible in the LDD data from Schiavon *et al.* [7] [∘ in Fig. 5(a)].

For blue emission, a strong increase of A with increasing defect density was reported previously [4,20]. However, most striking is that the difference in A of more than a factor of 10 between LDD and HDD vanishes towards longer wavelengths. Instead A increases on LDD LEDs by a factor of 10 from blue to green while A remains almost constant for HDD LEDs. Thus, on HDD LEDs, the nonradiative recombination A is likely limited by the dislocation density, which is wavelength independent, and A is insensitive to other nonradiative recombination centers with lower density.

The increase of A for LDD LEDs would indicate that there are other nonradiative recombination centers whose density increases towards the green. Indeed, Langer *et al.* directly observed a shortening of the nonradiative lifetime towards green [9] (⊠ in Fig. 5). The increase was even stronger than for our data, which may be related to thinner QWs in their experiment. Langer *et al.* attributed the increase of nonradiative recombination to strain. An increase in the nonradiative A coefficient was also reported for laser structures by Strauß *et al.* [8] which they attributed to a reduced “QW quality” from blue to green.

The higher growth temperatures of blue QWs versus green would reduce point-defect density (like carbon and vacancies). Indeed, two reports showed a strong increase of PL when increasing the QW growth temperature while keeping the same emission wavelength [10,11]. The PL IQE curves in Hammersley *et al.* also show the maximum IQE is reached at lower powers for higher QW growth temperatures [10], which directly confirms smaller A coefficients at lower QW growth temperatures. A recent deep-level optical spectroscopy study found in green QWs about 10 times more deep levels roughly 1.5 eV below the gap than for blue QWs, and at the same time a later peak in PL-IQE, i.e., a higher A coefficient [38]. This deep level seems related to the lowest deep level which increased in HDD QWs [6], which corresponds with our observation of A for LDD green LEDs similar to A for all HDD LEDs. For single QWs on Si substrate (and thus with TDDs between LDD and HDD) a direct correlation between deep levels and high A coefficients has been demonstrated (unfortunately, no emission wavelengths were given) [32]. Finally, a recent calculation of Shockley-Read-Hall recombination of 10^{16} cm^{-2} gallium vacancy-oxygen complexes [35] agrees very well with our observed increase of the A coefficient towards 500 nm (black dashed line in Fig. 5). However, at longer wavelength, the energy difference to nonradiative states is no longer the nonradiative recombination rate limiting factor and saturates. This again indicates towards an increasing number of point defects beyond 500 nm.

Thus, the increase of A towards green for LDD LEDs is most likely caused by an enhanced nonradiative recombination at a deep level originating from point defects (e.g., carbon or vacancies) which are more incorporated at the lower growth temperatures needed for green QWs.

The B coefficients roughly follow the calculated squared wave-function overlap of 3.0 nm (In,Ga)N QWs for all dislocation densities [line in Fig. 5(b)]. In the case of B two main competing mechanisms can either increase or reduce the radiative recombination, depending on the current density around the peak IQE used for the fitting.

The hole degeneracy decreases B for current densities exceeding typically 100 A cm^{-2} [23]. But those current densities are higher than the peak EQE (see Fig. 2). On the other hand, the screening of the internal fields at higher carrier densities increases the wave-function overlap [31,36] and thus B. Assuming that all carriers in a QW contribute to screening, one can calculate the carrier density at peak IQE from Eq. (8) and can then compare this to the calculated carrier density needed for a 10% change of the overlap for 3 nm QWs. The results in Fig. 6 show that all but one HDD LED device at 448 nm is below a limit of 10% increase of wave-function overlap. Thus, the B coefficient obtained from fitting is hardly affected by screening below the peak IQE.

At very high currents the carrier density can reach much higher values. The typical operation point of 350 mA for a green LDD LED is equivalent to a carrier density of $n \approx 4 \times 10^{18}$ cm^{-3} using the values from Fig. 5. This would increase the calculated overlap by 23% and via the square B by 50% while blueshifting the calculated emission by reasonable 8 nm. A comparable wavelength shift from peak EQE to maximum current was recently

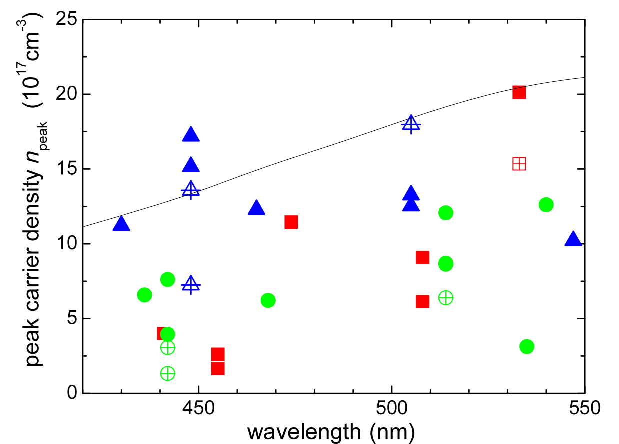

FIG. 6. Carrier densities $n_{\mathrm{peak}} = \sqrt{A/C}$ at peak IQE for all LEDs and the calculated carrier density for a 10% increase of the wave-function overlap (line).

reported for long-wavelength LEDs [39], supporting this estimation. Because B is low in the green region, carriers recombine slowly and accumulate more than in blue. The so-increased carrier density and thus screening can explain the observed broadening of the EQE curves at the highest current densities observed in Fig. 2 for the green LEDs.

Overall, we can confirm the results of Schiavon *et al.* that the B coefficient scales proportional to the squared wave-function overlap [7]. Dislocations as well as point defects have no big effect on the B coefficient: the radiative recombination only depends on the QW thickness and In content.

C. Modeling

From Fig. 5 we have obtained an ideal trend of the A, B, and C coefficients for low and high TDDs. With Eq. (6) we can then calculate the $\mathrm{IQE}_{\mathrm{peak}}$ for ideal devices.

For HDD, we keep A constant at $2 \times 10^7\ \mathrm{s}^{-1}$. For such a high A coefficient, the change of B due to the squared wave-function overlap is enough to explain the reduction of the peak IQE from 90% at 400 nm to 23% at 540 nm in Fig. 7(a). Thus, for high dislocation densities the green gap is indeed caused by the reduced wave-function overlap.

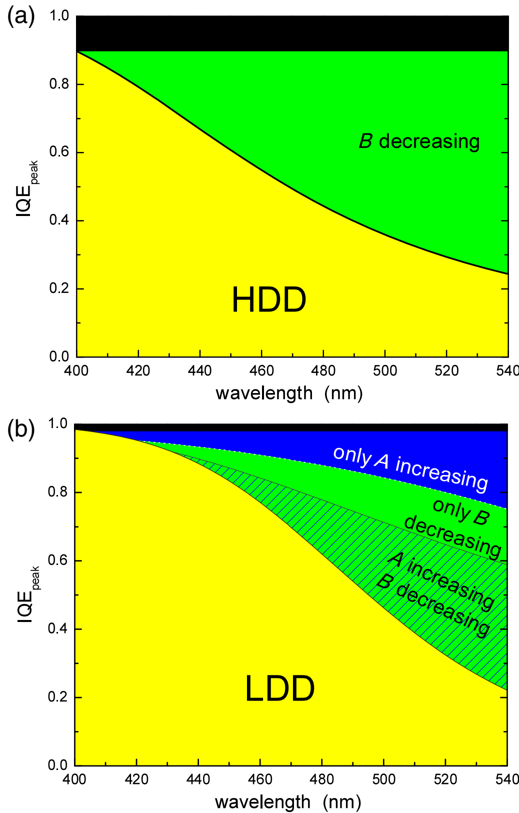

FIG. 7. Calculated peak IQE (solid) from Eq. (6) using the coefficients from Fig. 5 for (a) HDD LEDs with a fixed $A = 2 \times 10^7\ \mathrm{s}^{-1}$ and (b) LDDs LEDs.

However, when the A coefficient is much lower at the best LDD values of $10^6\ \mathrm{s}^{-1}$ [“only B decreasing” in Fig. 7(b)] then the peak IQE reduces much less, from 95% to 58%. If B is left unchanged at $10^{-10}\ \mathrm{cm}^3\,\mathrm{s}^{-1}$ (the 420 nm value) and only A increases according to Fig. 5(a), then the peak IQE reduces from 95% to 75% [“only A increasing” in Fig. 7(b)]. Only if both A increases and B decreases, then the peak IQE reduces from 95% at 400 nm to 22% at 540 nm, the typical values reported in literature (cf. EQE at 20 mA in Refs. [40,41]).

Hence, the reduction of the IQE towards green on low dislocation templates is not only caused by the reduction of the wave-function overlap (i.e., radiative recombination B), but it is also due to a strong increase of A. In other words, a nonradiative recombination at defects, most likely point defects, is a strong contribution to the reduction of the IQE towards green, whereas dislocations even in the $10^9\ \mathrm{cm}^{-3}$ range do not limit the IQE in the green. This is supported by a recent publication which showed that the growth temperature of a QW strongly affects the IQE as measured by photoluminescence [10]. Furthermore, the deep-level signals in spectroscopy typical for HDD are also reached on LDD by QW grown at a lower temperature to incorporate more In [6,38]. If we could produce green QWs with a similar nonradiative recombination rate as for blue QWs, then a peak IQE close to 60% would be possible even for green QWs [shaded area in Fig. 7(b)].

IV. CONCLUSION

From measuring the EQE curves of LEDs with different defect densities which emit from 450 to 540 nm, we conclude that dislocations mainly increase the nonradiative recombination in the blue wavelength region. The radiative recombination follows the calculated squared wave-function overlap. Using the experimental ABC coefficients to model LEDs with different dislocation densities strongly suggests that nonradiative recombination is an important factor to the green gap. Hence, the performance of green LEDs cannot be improved to match that of blue LEDs only by reducing the polarization fields. Point defects and other sources of nonradiative recombination must also be addressed.

ACKNOWLEDGMENTS

This work is supported by U.K. Engineering and Physics Scientific Research Council Grants No. EP/K008323/1 and No. EP/I012591/1.

[1] Martin F. Schubert, Sameer Chhajed, Jong Kyu Kim, E. Fred Schubert, Daniel D. Koleske, Mary H. Crawford, Stephen R. Lee, Arthur J. Fischer, Gerald Thaler, and Michael A. Banas, Effect of dislocation density on

efficiency droop in GaInN/GaN light-emitting diodes, Appl. Phys. Lett. **91**, 231114 (2007).

[2] X. A. Cao, Y. Yang, and H. Guo, On the origin of efficiency roll-off in InGaN-based light-emitting diodes, J. Appl. Phys. **104**, 093108 (2008).

[3] Z. Liu, T. Wei, E. Guo, X. Yi, L. Wang, J. Wang, G. Wang, Y. Shi, I. Ferguson, and J. Li, Efficiency droop in InGaN/GaN multiple-quantum-well blue light-emitting diodes grown on free-standing GaN substrate, Appl. Phys. Lett. **99**, 091104 (2011).

[4] Shigeya Kimura, Jumpei Tajima, Hajime Nago, Toshiki Hikosaka, Hisashi Yoshida, Kenjiro Uesugi, and Shinya Nunoue, Optical properties of InGaN/GaN MQW LEDs grown on Si (111) substrates with low threading dislocation densities, Proc. SPIE Int. Soc. Opt. Eng. **8986**, 89861H (2014).

[5] Yoshiyuki Harada, Toshiki Hikosaka, Shigeya Kimura, Maki Sugai, Hajime Nago, Koichi Tachibana, Naoharu Sugiyama, and Shinya Nunoue, Effect of dislocation density on efficiency curves in InGaN/GaN multiple quantum well light-emitting diodes, Proc. SPIE Int. Soc. Opt. Eng. **8278**, 82780J (2012).

[6] A. Armstrong, T. A. Henry, D. D. Koleske, M. H. Crawford, K. R. Westlake, and S. R. Lee, Dependence of radiative efficiency and deep level defect incorporation on threading dislocation density for InGaN/GaN light emitting diodes, Appl. Phys. Lett. **101**, 162102 (2012).

[7] Dario Schiavon, Michael Binder, Matthias Peter, Bastian Galler, Philipp Drechsel, and Ferdinand Scholz, Wavelength-dependent determination of the recombination rate coefficients in single-quantum-well GaInN/GaN light emitting diodes, Phys. Status Solidi (b) **250**, 283 (2013).

[8] Uwe Strauß, Thomas Hager, Georg Brüderl, Teresa Wurm, André Somers, Christoph Eichler, Clemens Vierheilig, Andreas Löffler, Jelena Ristic, and Adrian Avramescu, Recent advances in *c*-plane GaN visible lasers, Proc. SPIE Int. Soc. Opt. Eng. **8986**, 89861L (2014).

[9] Torsten Langer, Holger Jönen, Andreas Kruse, Heiko Bremers, Uwe Rossow, and Andreas Hangleiter, Strain-induced defects as nonradiative recombination centers in green-emitting GaInN/GaN quantum well structures, Appl. Phys. Lett. **103**, 022108 (2013).

[10] S. Hammersley, M. J. Kappers, F. C.-P. Massabuau, S.-L. Sahonta, P. Dawson, R. A. Oliver, and C. J. Humphreys, Effects of quantum well growth temperature on the recombination efficiency of InGaN/GaN multiple quantum wells that emit in the green and blue spectral regions, Appl. Phys. Lett. **107**, 132106 (2015).

[11] Chi-Feng Huang, Tzu-Chi Liu, Yen-Cheng Lu, Wen-Yu Shiao, Yung-Sheng Chen, Jyun-Kai Wang, Chih-Feng Lu, and C. C. Yang, Enhanced efficiency and reduced spectral shift of green light-emitting-diode epitaxial structure with prestrained growth, J. Appl. Phys. **104**, 123106 (2008).

[12] S. Das Bakshi, J. Sumner, M. J. Kappers, and R. A. Oliver, The influence of coalescence time on unintentional doping in GaN/sapphire, J. Cryst. Growth **311**, 232 (2009).

[13] R. A. Oliver, M. J. Kappers, J. Sumner, R. Datta, and C. J. Humphreys, Highlighting threading dislocations in MOVPE-grown GaN using an *in situ* treatment with SiH_4 and NH_3, J. Cryst. Growth **289**, 506 (2006).

[14] R. A. Oliver, F. C. -P. Massabuau, M. J. Kappers, W. A. Phillips, E. J. Thrush, C. C. Tartan, W. E. Blenkhorn, T. J. Badcock, P. Dawson, M. A. Hopkins, D. W. E. Allsopp, and C. J. Humphreys, The impact of gross well width fluctuations on the efficiency of GaN-based light emitting diodes, Appl. Phys. Lett. **103**, 141114 (2013).

[15] F. C. -P. Massabuau, M. J. Davies, F. Oehler, S. K. Pamenter, E. J. Thrush, M. J. Kappers, A. Kovács, T. Williams, M. A. Hopkins, C. J. Humphreys, P. Dawson, R. E. Dunin-Borkowski, J. Etheridge, D. W. E. Allsopp, and R. A. Oliver, The impact of trench defects in InGaN/GaN light emitting diodes and implications for the "green gap" problem, Appl. Phys. Lett. **105**, 112110 (2014).

[16] Markus Pristovsek, Wavelength limits for InGaN quantum wells on GaN, Appl. Phys. Lett. **102**, 242105 (2013).

[17] Han-Youl Ryu, Hyun-Sung Kim, and Jong-In Shim, Rate equation analysis of efficiency droop in InGaN light-emitting diodes, Appl. Phys. Lett. **95**, 081114 (2009).

[18] Qi Dai, Qifeng Shan, Jing Wang, Sameer Chhajed, Jaehee Cho, E. Fred Schubert, Mary H. Crawford, Daniel D. Koleske, Min-Ho Kim, and Yongjo Park, Carrier recombination mechanisms and efficiency droop in GaInN/GaN light-emitting diodes, Appl. Phys. Lett. **97**, 133507 (2010).

[19] Bastian Galler, Hans-Jürgen Lugauer, Michael Binder, Richard Hollweck, Yannick Folwill, Anna Nirschl, Alvaro Gomez-Iglesias, Berthold Hahn, Joachim Wagner, and Matthias Sabathil, Experimental determination of the dominant type of Auger recombination in InGaN quantum wells, Appl. Phys. Express **6**, 112101 (2013).

[20] Y. C. Shen, G. O. Mueller, S. Watanabe, N. F. Gardner, A. Munkholm, and M. R. Krames, Auger recombination in InGaN measured by photoluminescence, Appl. Phys. Lett. **91**, 141101 (2007).

[21] Stefan Schulz, Miguel A. Caro, Conor Coughlan, and Eoin P. O'Reilly, Atomistic analysis of the impact of alloy and well-width fluctuations on the electronic and optical properties of InGaN/GaN quantum wells, Phys. Rev. B **91**, 035439 (2015).

[22] A. Morel, P. Lefebvre, S. Kalliakos, T. Taliercio, T. Bretagnon, and B. Gil, Donor-acceptor-like behavior of electron-hole pair recombinations in low-dimensional $(\mathrm{Ga,In})N/\mathrm{GaN}$ systems, Phys. Rev. B **68**, 045331 (2003).

[23] Sergey Karpov, ABC-model for interpretation of internal quantum efficiency and its droop in III-nitride LEDs: A review, Opt. Quantum Electron. **47**, 1293 (2015).

[24] T. J. Badcock, M. Ali, T. Zhu, M. Pristovsek, R. A. Oliver, and A. J. Shields, Radiative recombination mechanisms in polar and non-polar InGaN/GaN quantum well LED structures, Appl. Phys. Lett. **109**, 151110 (2016).

[25] Aurelien David, Christophe A. Hurni, Nathan G. Young, and Michael D. Craven, Carrier dynamics and Coulomb-enhanced capture in III-nitride quantum heterostructures, Appl. Phys. Lett. **109**, 033504 (2016); Erratum, Appl. Phys. Lett. **109**, 033504 (2016); **109**, 099902 (2016).

[26] Felix Nippert, Sergey Karpov, Ines Pietzonka, Bastian Galler, Alexander Wilm, Thomas Kure, Christian Nenstiel, Gordon Callsen, Martin Straßburg, Hans-Jürgen Lugauer, and Axel Hoffmann, Determination of recombination coefficients in InGaN quantum-well light-emitting diodes by small-signal time-resolved photoluminescence, Jpn. J. Appl. Phys. **55**, 05FJ01 (2016).

[27] J. Hader, J. V. Moloney, and S. W. Koch, Density-activated defect recombination as a possible explanation for the efficiency droop in GaN-based diodes, Appl. Phys. Lett. **96**, 221106 (2010).

[28] Hongping Zhao, Guangyu Liu, Ronald A. Arif, and Nelson Tansu, Current injection efficiency induced efficiency-droop in InGaN quantum well light-emitting diodes, Solid State Electron. **54**, 1119 (2010).

[29] Aurelien David, Christophe A. Hurni, Nathan G. Young, and Michael D. Craven, Electrical properties of III-nitride LEDs: Recombination-based injection model and theoretical limits to electrical efficiency and electroluminescent cooling, Appl. Phys. Lett. **109**, 083501 (2016).

[30] C. van Opdorp and G. W. 't Hooft, Method for determining effective nonradiative lifetime and leakage losses in double-heterostructure lasers, J. Appl. Phys. **52**, 3827 (1981).

[31] Petr G. Eliseev, Marek Osin'ski, Hua Li, and Irina V. Akimova, Recombination balance in green-light-emitting GaN/InGaN/AlGaN quantum wells, Appl. Phys. Lett. **75**, 3838 (1999).

[32] C. De Santi, M. Meneghini, M. La Grassa, B. Galler, R. Zeisel, M. Goano, S. Dominici, M. Mandurrino, F. Bertazzi, D. Robidas, G. Meneghesso, and E. Zanoni, Role of defects in the thermal droop of InGaN-based light emitting diodes, J. Appl. Phys. **119**, 094501 (2016).

[33] Matteo Meneghini, Nicola Trivellin, Gaudenzio Meneghesso, Enrico Zanoni, Ulrich Zehnder, and Berthold Hahn, A combined electro-optical method for the determination of the recombination parameters in InGaN-based light-emitting diodes, J. Appl. Phys. **106**, 114508 (2009).

[34] Junjun Wang, Tobias Meisch, Dominik Heinz, Raphael Zeller, and Ferdinand Scholz, Internal quantum efficiency and carrier injection efficiency of *c*-plane, $(11\bar{1}2)$ and $(10\bar{2}2)$ InGaN/GaN-based light-emitting diodes, Phys. Status Solidi (b) **253**, 174 (2016).

[35] Audrius Alkauskas, Cyrus E. Dreyer, John L. Lyons, and Chris G. Van de Walle, Role of excited states in Shockley-Read-Hall recombination in wide-band-gap semiconductors, Phys. Rev. B **93**, 201304 (2016).

[36] Richard P. Green, Jonathan J. D. McKendry, David Massoubre, Erdan Gu, Martin D. Dawson, and A. E. Kelly, Modulation bandwidth studies of recombination processes in blue and green InGaN quantum well micro-light-emitting diodes, Appl. Phys. Lett. **102**, 091103 (2013).

[37] Aurélien David and Michael J. Grundmann, Droop in InGaN light-emitting diodes: A differential carrier lifetime analysis, Appl. Phys. Lett. **96**, 103504 (2010).

[38] Andrew M. Armstrong, Mary H. Crawford, and Daniel D. Koleske, Contribution of deep-level defects to decreasing radiative efficiency of InGaN/GaN quantum wells with increasing emission wavelength, Appl. Phys. Express **7**, 032101 (2014).

[39] Shinji Saito, Rei Hashimoto, Jongil Hwang, and Shinya Nunoue, InGaN light-emitting diodes on *c*-face sapphire substrates in green gap spectral range, Appl. Phys. Express **6**, 111004 (2013).

[40] Liu Jun-Lin, Zhang Jian-Li, Wang Guang-Xu, Mo Chun-Lan, Xu Long-Quan, Ding Jie, Quan Zhi-Jue, Wang Xiao-Lan, Pan Shuan, Zheng Chang-Da, Wu Xiao-Ming, Fang Wen-Qing, and Jiang Feng-Yi, Status of GaN-based green light-emitting diodes, Chin. Phys. B **24**, 067804 (2015).

[41] Markus Pristovsek, Colin J. Humphreys, Sebastian Bauer, Manuel Knab, Klaus Thonke, Grzegorz Kozlowski, Donagh O'Mahony, Pleun Maaskant, and Brian Corbett, Comparative study of (0001) and $(10\bar{2}2)$ InGaN based light emitting diodes, Jpn. J. Appl. Phys. **55**, 05FJ10 (2016).